Wetting of porous thin films exhibiting large contact angles

L.E. Helseth and M.M. Greve

Department of Physics and Technology, Allegaten 55, 5020 Bergen, University of Bergen, Norway

Email: Lars.Helseth@uib.no

ABSTRACT: Porous solid films which promote large apparent contact angles are interesting systems since the wetting properties are dependent on both surface structure and water penetration into the film. In this study, a parahydrophobic coating is made by sequential dip-coating of titanium dioxide nanoparticles and stearic acid on polished copper substrates. The apparent contact angles are determined using the tilted plate method, and it is found that the liquid-vapor interaction decreases and water droplets are more likely to move off the film when the number of coated layers increase. Interestingly, it is found that under some conditions the front contact angle can be smaller than the back contact angle. Scanning electron microscopy observations demonstrate that the coating process led to formation of hydrophilic TiO_2 nanoparticle domains and hydrophobic stearic acid flakes which allow heterogeneous wetting. By monitoring electrical current through the water droplet to the copper substrate, it is found that the water drops penetrate the coating layer to make direct contact with the copper surface with a time delay and magnitude that depends on the coating thickness. This additional penetration of water into the porous film enhances the adhesion of the droplet to the film and provides a clue to understand the contact angle hysteresis.

KEYWORDS: Wetting, parahydrophobic film, porous surface, electrical current

1. Introduction

Surfaces with different types of wettability can be created in a variety of manners [1], in many cases inspired by Nature itself [2]. Surfaces which give rise to large apparent contact angle (>150˚) and low sliding angle (<10°) of water droplets are referred to as superhydrophobic and may be applied to self-cleaning surfaces. Surfaces which exhibit large apparent contact angle and high sliding angles are referred to as parahydrophobic [3,4], and may have importance in for example printing and liquid transfer [5].

Surface roughness plays an important role in wetting [6-8]. Large contact angles can be obtained using hierarchical structures, with both micro and nanoscale features, were the surface energy has been lowered by chemical agents [9-12]. Some of these chemical agents are highly effective, but they require much energy to produce and their release into Nature should be avoided. For these reasons, there is ongoing research to find solutions which have the smallest environmental footprint. Nanocoatings of TiO_2 or other oxides onto rock allows one to obtain controllable oleophobicity and hydrophilicity [13,14]. Amongst the available environmentally friendly materials for lowering the surface energy, it appears that stearic acid has gained popularity as a cost-effective and biocompatible choice. Stearic acid can be applied to different engineering materials [15-20] and nanostructured surfaces [21] for obtaining surfaces with large apparent contact angle (>150°) and variable sliding angle. A system of stearic acid and either Al_2O_3, TiO_2 or SiO_2 appears attractive, since these particles are readily available and applicable to a range of materials. Recent studies have demonstrated that dip coating layers of Al_2O_3 nanoparticles and stearic acids provide large contact angle surfaces which protect wood from water [22], while TiO_2 nanoparticles combined with stearic acid may provide stable hydrophobic coating also on cloth fibers [23,24]. However, further studies are needed to understand how simple and economical methods, such as dip coating, can be used to obtain parahydrophobic surfaces.

For strongly adhering droplets, contact angle hysteresis plays and important role, and has been reviewed in recent reports [25,26]. Contact angle hysteresis measurements often start by deposition of a droplet on the surface of interest, and then injecting volume until the contact line just starts to advance. This is called

the advancing contact angle. A similar reduction of volume of a deposited droplet allows one to find the receding contact angle. The difference between the advancing and receding contact angles is often called contact angle hysteresis. Another technique for finding the contact angle hysteresis uses the tilted plate method [27-29]. Here, the droplet is tilted until the gravitational pull becomes so large that the droplet slides or rolls off the sample surface. Just when this happens, one records the contact angle of the front and back of the droplet (advancing and receding contact lines) and call the difference between them contact angle hysteresis. Since both methods typically rely on optical imaging where the microscopic features of the water surface are not observed directly, both these methods result in apparent contact angles, and therefore apparent contact angle hysteresis as discussed in Ref. [25]. However, the two techniques are also accessing different information about the surface, as they use different deposition methods (injection versus tilting) and different forces (pressure due to volume injection versus droplet deformation due to tilting) to create droplet motion. Moreover, if the water droplets are exposed to large adhesion forces one may not be able to move the droplets off the surface at all. The droplets may interact with not only the upper surface, but also penetrate into pores if these are accessible, thus controlling the adhesion as well.

In the current study, we used the tilted plate method to determine the contact angle. In this method, the tilting causes the gravitational force to change direction relative to the coating surface, thus altering ability to penetrate into the porous network in the front and the back of the droplet. This is highly advantageous if one is interested in observing the hysteretic behavior of the water drop on the porous coating, and allows one to interpret the liquid-vapor interaction in a manner inaccessible to volume-injection techniques. Furthermore, the tilted plate method avoids the difficulty of interpreting results related to volume rate-dependent penetration of droplets into the network that would be the result if one were to obtain the advancing and receding contact angles using volume injections. By complementing the contact angle measurements with electrical current measurements through the porous network, it is studied how the water penetrates the coating layer to make direct contact with the copper surface and how this process

depends on the number of coating layers used. This combination of measurement techniques allows one to obtain a better understanding of the correlation between the wetting and water penetration, and may guide more precise designs of coatings which retain and transfer water in the form of droplets.

2. Materials and methods

Materials: TiO_2 nanoparticles (718467-100G, Lot # MKBL0267V), stearic acid (reagent grade, 95%, 175366-1KG, Lot # MKBX7640V) and methanol (puriss, 32213-1L Lot# SZBA2440V) were purchased from Sigma Aldrich. As substrates, 0.5 mm thick copper plates were used. The copper surface was polished with silicon carbide abrasive paper of grit size P1200, thus generating surface roughness mean size of about 15 μm.

Preparation of layered film: Two solutions for the dipcoating was prepared. First, 20 mM stearic acid was prepared in methanol under vigorous stirring until all the solid dissolved in a glass container. Secondly, 0.2 g TiO_2 nanoparticles was dispersed in 10 mL methanol and placed in a heated water bath and ultrasonicated for 30 min in a second container. The experimental procedure for creating the layered films is summarized in Fig. 1. First, the polished copper substrate is submerged in the solution containing TiO_2 nanoparticles for 30 seconds and subsequently air-dried until the surface appeared entirely dry (about 5 min). Next, the nanoparticle-coated copper surface was immersed in stearic acid, and subsequently dried (about 5 min). In this way one layer (N=1) of coating composed of nanoparticles and stearic acid was created. The procedure was repeated for N=1, 2, 3, 5 and 7 layers. All surfaces studied here were terminated by stearic acid dip coating in order to ensure that the surface had large contact angle. All coating procedures and subsequent characterization has been conducted in ambient air and room temperature (between 19 and 22 °C).

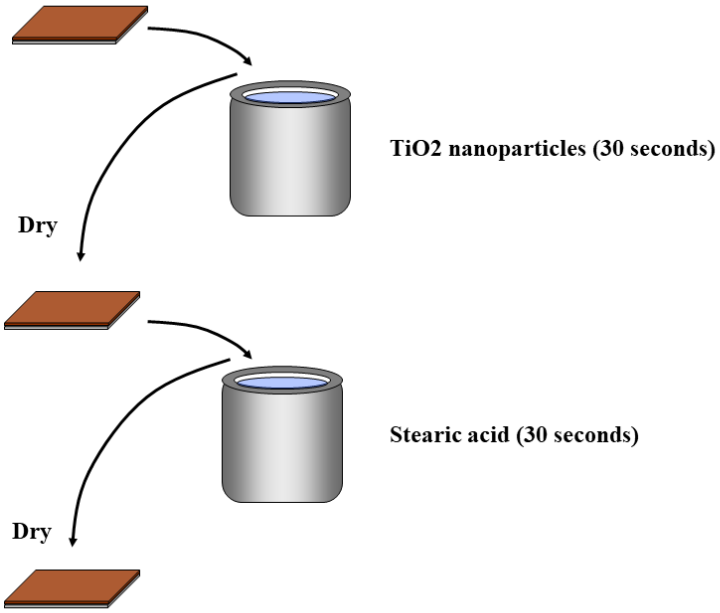

Figure 1. Experimental procedure for dip coating the polished copper samples.

Scanning Electron Microscopy: The surface morphology and to some extent the topography of the samples was investigated using Scanning Electron Microscopy (Raith eLine). SEM images of the samples were captured from directly above, and the system was optimized for reduced sample charging during imaging [30]. Typical images of an N=5 layer structure, obtained using acceleration voltage 10 kV, are shown in fig. 2. From Fig. 2 b) and similar figures it was found that the diameter of the TiO_2 particles was 34 ± 15 nm, which is within the range (mean diameter 21 nm) given by the manufacturer. Further SEM images of the film structure, TiO_2 nanoparticle and stearic acid domains are given for N=1,3,5 and 7 in Figs. S1, S2 and S3 in the supplementary material.

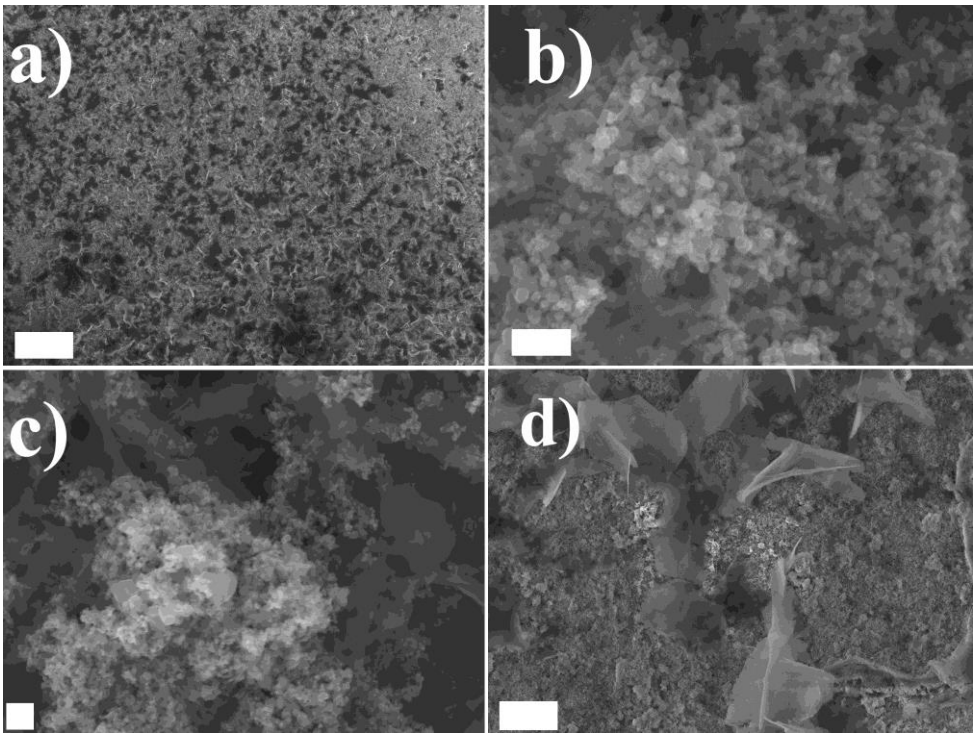

Figure 2. SEM images of the TiO_2+stearic acid structure (with N=5 layers). The stearic acid is seen as thin flakes in the micrographs, perhaps most clearly in d). The scalebar in a) is 200 μm, whereas in b) and c) it is 200 nm and in d) 20 μm.

Contact angle measurements: The wetting of nanostructured films by deionized water drops (Millipore, 18.2 MΩcm) was studied using an OCA 20L contact angle measurement system in a tilted plate mode. The tilted plate method allows one to record contact angles of a droplet deposited on a surface tilted such that it is no longer aligned perpendicular to the gravitational field, thus allowing one to obtain information about drop retention [27,28]. It is known that the particular droplet deposition method may influence the results of a tilted plate experiment, and the observed maximum and minimum observed contact angles do not necessarily represent the advancing and receding angles [28]. However, the tilted plate method does give a better understanding of actual retention of a drop on a surface and is therefore favorable for some practical applications where large contact angle hysteresis is present. In the current study, a syringe was placed close to the horizontally aligned surface and drops of volume 5 μL were gently placed in contact

with the surface. Due to the vertical droplet-surface attraction, the drops would adhere to the surface. A motor was used to slowly change the tilt angle, and a camera system recorded images of the water droplets. The camera software allows one to extract the contact angle of the back (left) and front (right) parts of the droplets, see Fig. 3.

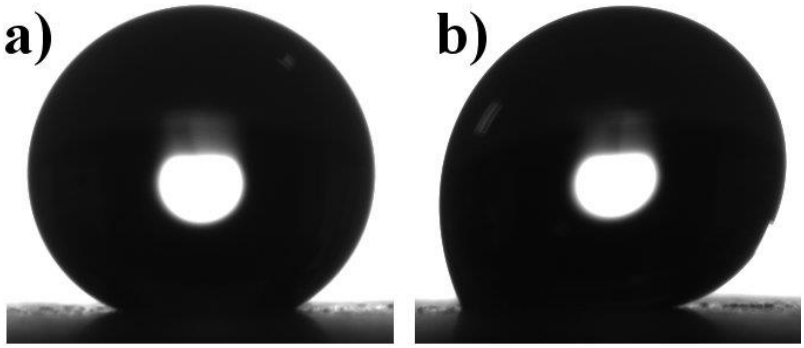

Figure 3. A 5 μL water drop on a 5-layered structure for tilting angles α=0° (a) and α=90° (b).

The sequence and time used for the tilting plate experiment was kept the same in every experiment. The substrate was tilted gradually while recording the contact angles on the left and right sides, until the tilting angle reached α=90°. An example of this is seen in fig. 3 b), where the contact angle on the back side (left hand side) is θ_b=108°, whereas that on the front side (right hand side) is θ_f=160°. When the tilting angle has reached α=90°, it is again gradually returned to α=0° while continuing to record the left and right contact angles. Figure 3 a) shows a typical image of the droplet when the stage first was tilted to an angle α=90° and then back again to α=0°. Here the contact angle on the back side (left hand side) is θ_b = 157°, whereas that on the front side (right hand side) is θ_f=151°. Different values for the back and front contact angles at α=0° is due to local environment at the particular position of the contact line perimeter and will be considered in more detail later.

The whole procedure measuring contact angles took much less time than that required to evaporate the drop (i.e. the drop diameter changed by maximum a few percent). For each drop, the measurements were repeated a second time at the same location to improve the measurement statistics. Moreover, additional measurements were carried out on at least three different locations on each sample.

Electrical characterization: The penetration of water through the nanostructured films was monitored using current transients. A drop of volume about 100 μL was placed on top of the polished copper substrate coated with TiO_2 and stearic acid. A copper surface with coating connected to a micrometer screw stage approached from above to touch the upper cap of the water drop in the same position every time. Current transients were recorded with a water droplet resting on a bare copper electrode, before and after the other copper electrode coated with TiO_2 and stearic acid approached from above to contact the droplet. The voltage was maintained at 0.5 V, while the current transient was monitored by a Keithley 6514 current measurement system. A schematic drawing of the experimental setup is shown in Fig. 4.

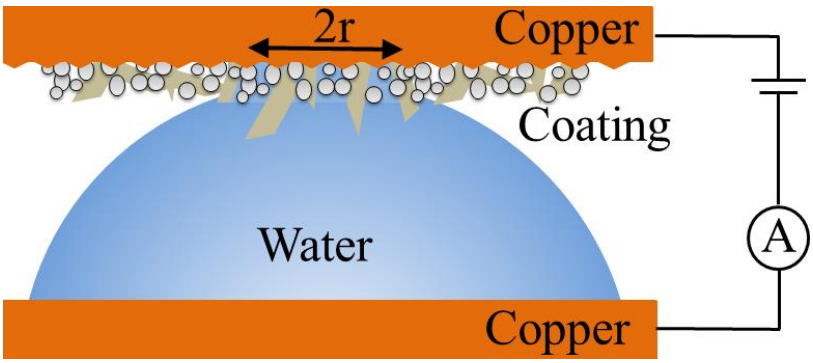

Figure 4. Schematic drawing of setup for electrical measurements of water penetration through the coating.

3. Contact angle hysteresis

It is well-known in the literature that the advancing and receding contact angles may differ from the measured front and rear contact angles [25,28]. Receding of contact angles on microscale well-defined [31] and irregular structures [32] have revealed that stepwise depinning plays a major role in the dynamics of wetting. Many studies have been undertaken to investigate wetting on rough heterogenous surfaces, where the perhaps most known theories are related to Cassie and Wenzel's laws [6-8,33,34].

Here, we will adopt a modification of the force-balance-approach considered in refs. [35,36], wherein one despite the heterogeneity and microscopic surface roughness assume average forces as seen in fig. 5. For simplicity, one distinguishes between the back and forth of the water drop, since here the friction force working against gravity must point out of and into the drop, respectively. At any instant, the average apparent contact angle of the back part of the droplet is θ_b, whereas that of the front part is θ_f, see fig. 5.

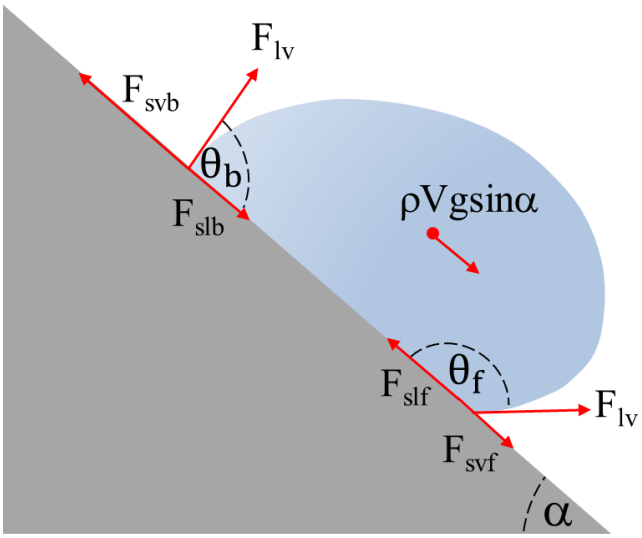

Figure 5. Schematic drawing of the external forces acting on a tilted drop. See text for explanation.

For the backside of the water drop on a surface, there are three forces at the three-phase contact line, namely the force due to solid-vapor interaction (F_{svb}), the force due to solid-liquid interaction (F_{slb}), and the force due to liquid-vapor interaction (F_{lv}). For a drop at rest when the tilt angle is α=0, one has $F_{svb}=F_{slb}+F_{lv}\cos\theta_b$, as required by balancing the forces. Tilting may or may not result in spatial shifting of the contact line, with or without depinning. In any case, the solid-liquid force (F_{slb}), the solid-vapor force (F_{svb}) and the contact angle θ_b may change. For the front part of the contact line, the average solid-liquid force (F_{slf}), the solid-vapor force (F_{svf}) and the contact angle θ_f may also change when the droplet is tilted. However, we will here make the simplifying assumption that the liquid-vapor interaction force (F_{lv}) remains unchanged for both the front and back parts of the contact line during tilting. While this assumption appears reasonable if one assumes that the solid surface does not influence the liquid-vapor interactions, its verification through studies of microscopic details is outside the scope of the current study.

Using the forces drawn in fig. 5 and Newtons 2nd law, the friction force is balanced against the gravitational force parallel to the coating, $\rho V g \sin\alpha$, such that

$$\cos\theta_b - \cos\theta_f = \frac{\rho V g \sin\alpha}{F_{lv}} + \frac{\Delta F}{F_{lv}} \quad , \qquad (1)$$

where $\Delta F=(F_{svf}-F_{svb})+(F_{slb}-F_{slf})$ is a measure of the difference in solid-vapor and solid-liquid forces between the front and the back of the drop for a given tilt angle α. The information about roughness is hidden within F_{lv} and ΔF, and will not be considered explicitly here since we do not have available an instrument to accurately distinguish the contact line in contact with either air or solid on a microscopic scale. Clearly, the approach given here assumes averaging over the contact line perimeter for the front and back parts of the drop. In principle, ΔF may depend on the tilt angle, but it may also depend on the particular position on the substrate. However, if the contact line perimeter samples enough positions on the substrate, one could regard ΔF as some sort of average which may only depend weakly on the tilt

angle and position on the substrate. A plot of the measurable quantity $\cos\theta_f - \cos\theta_b$ versus $\sin\alpha$ then allows one to extract the two parameters F_{lv} and ΔF.

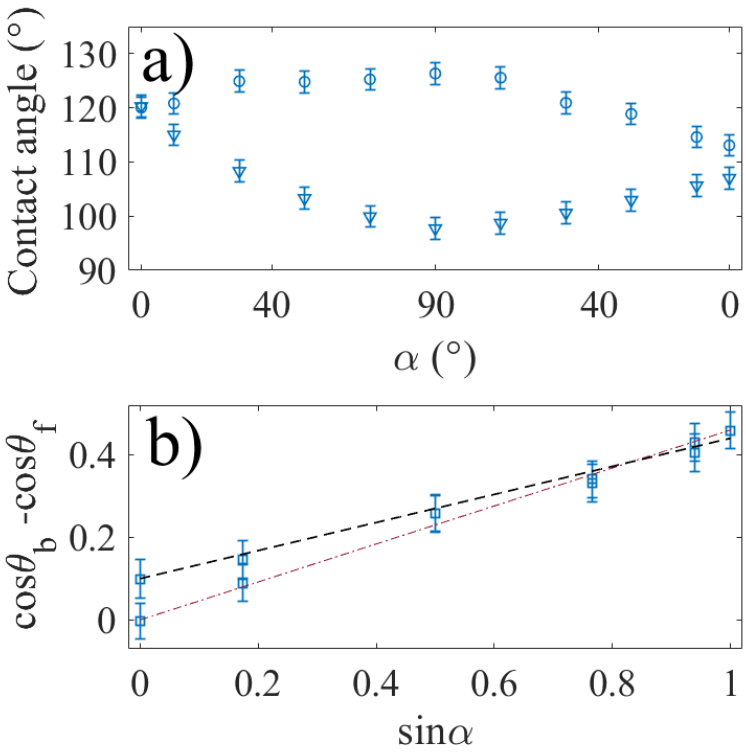

Figure 6. The contact angle hysteresis curve for a pure stearic acid coating. In a), the back (θ_b - triangles) and front (θ_f - circles) contact angles are shown as a function of tilt angle (a). In b), $\cos\theta_f - \cos\theta_b$ is plotted versus $\sin\alpha$ (squares), and the dashed and dash-dotted lines are fit to the experimental data. See text for details.

An example of experimental data showing θ_f (circles) and θ_b (triangles) as a function of the stage tilt angle is shown in Fig. 6 a) for a single layer of stearic acid. Here, the polished copper surface was dipped in stearic acid for 30 sec and dried, and since the coating is very thin it appears to be of comparable roughness to that of the bare copper substrate. The resulting coating is hydrophobic. From the data it is found that the initial contact angles at $\alpha = 0°$ are $\theta_f = \theta_b = 120 \pm 2°$, while the maximum difference in front and back contact angles is $\Delta\theta = 29 \pm 3°$ at $\alpha = 90°$. The advantage of representing the contact angle versus tilt as in

fig. 6 for hysteretic samples is twofold. First, it gives a visual impression of the initial and final contact angles and whether they are equal. The opening of the hysteresis 'eye' is a statement about the maximum difference in contact angles, thus indicating how well the droplets adhere to the sample. The skewness of the graph indicates how much the contact angles have changed while the droplets are tilted.

Figure 6 b) shows a plot of $\cos\theta_f - \cos\theta_b$ versus $\sin\alpha$. A linear fit starting from the origin (A=0) is shown as a dash-dotted brown line with $\rho Vg/F_{lv}=0.46$, and provides the best fit for the data when the tilt angle changes from $\alpha = 0°$ to $\alpha = 90°$. Here $\rho=1000$ kg/m^3, V=5 μL and g=9.8 N/kg, such that the gravity acting on a 5 μL drop is $\rho Vg=49$ μN. From fig. 6 a) it is clear that the back and front contact angles are not the same when the tilt angle once more goes back to zero, such that one has $A\neq 0$. The dashed line in Fig. 6 b) is a fit to these latter experimental data assuming $\Delta F/F_{lv} =0.1$ and $\rho Vg/F_{lv}=0.34$. These data suggest that the liquid-vapor force F_{lv} is 2-3 times larger than gravity, and that the difference in solid-vapor and solid-liquid forces between the front and the back of the drop is about one-tenth of the liquid-vapor force for a pure stearic acid coating. The fact that $\theta_b \approx \theta_f$ before the tilting experiment starts ($\alpha = 0°$) may indicate that the wetting properties are rather similar on both sides of the droplets, at least for the deposition method used here wherein the droplet is gently deposited vertically down on the substrate. However, after tilting the stage to $\alpha = 90°$, one observes that $\theta_f > \theta_b$ when one tilts back to $\alpha = 0°$. This is possibly due to gravity-induced rearrangement of the contact line into (pinned) metastable states as discussed in for example Ref. [4]. This observation also appears to agree with a recent study, emphasizing the entropic contribution favoring larger advancing than receding angles [37].

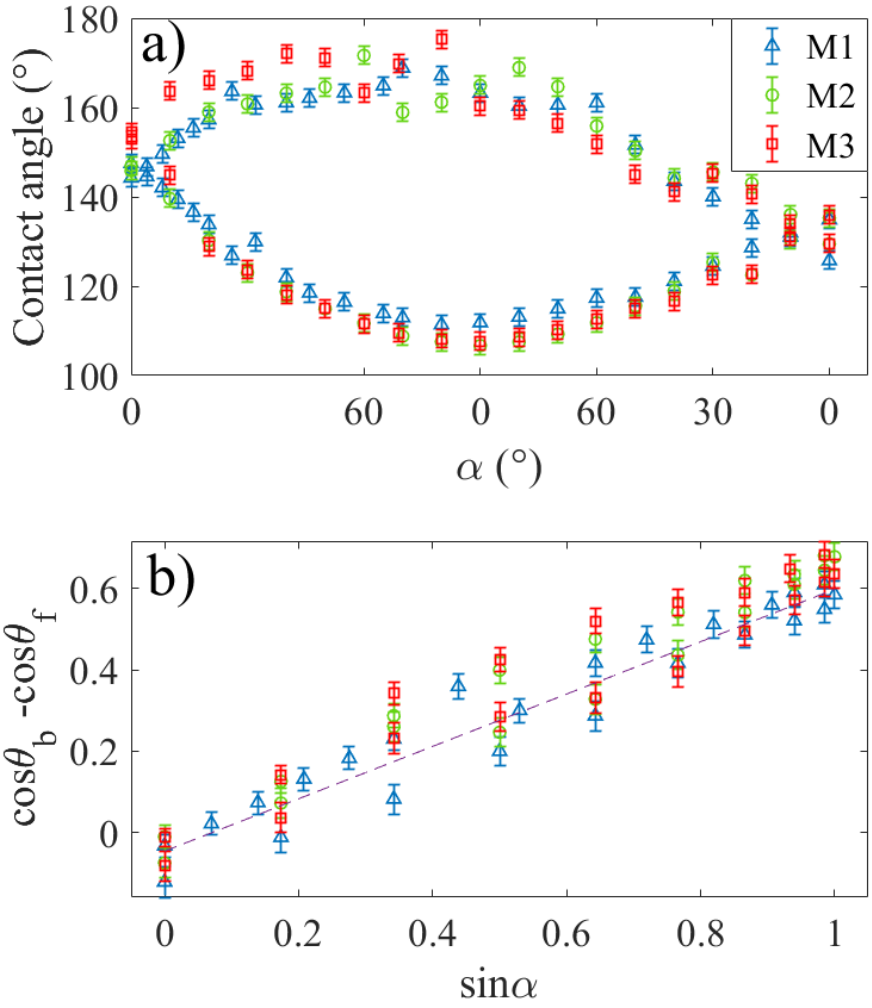

Figure 7. The contact angle hysteresis curve for N=1 layer of TiO_2+stearic acid for three different 5μL droplets taken on 3 different locations for each of the samples (a). In a), the back (θ_b – lower data points) and front (θ_f – upper data points) contact angles are shown as a function of tilt angle (a). Here M1 represent measurement series 1, M2 measurement series 2 and M3 measurement series 3, and the corresponding symbols (blue triangle, green circle and red square) are used in both a) and b). In b), $\cos\theta_f$ - $\cos\theta_b$ is plotted versus sinα for the data seen in a), and the dashed line is a fit of eq. (1) to the experimental data. See text for details.

Figure 7 a) shows the front and back contact angles as function of tilt angles for N=1 layer of TiO_2+stearic acid for three different 5μL droplets taken on 3 different locations for each of the samples. It is observed that the initial contact angles are about 150°, while the maximum difference in contact angle is $\Delta\theta = 59 \pm 5°$. Figure 7 b) shows a plot of $\cos\theta_f - \cos\theta_b$ versus $\sin\alpha$ for all the data in Fig. 7 a), while the dashed line is a fit of eq. (1) to the data using $\Delta F/F_{lv} = -0.05$ and $\rho Vg/F_{lv} = 0.64$. The liquid-vapor force F_{lv} has decreased to about 1.5 times the gravity, whereas ΔF, the difference in solid-vapor and solid-liquid forces between the front and the back of the drop, has switched sign as compared for a pure stearic acid.

For coatings made of pure stearic acid (fig. 6), N=1 (fig. 7) and N=2 layers (not shown), the 5 μL water droplets never moved off the surface for any tilting angle, which means that the friction force is able to be at least as large as the gravitational pull on the droplet, i.e. $\rho Vg = 49$ μN. However, for N equal to 5 or larger, this situation changed. Figure S4 a) in the supporting information shows the front and back contact angles as function of tilt angles for N=5 with four different droplets located at different positions. It is seen that two of the 5 μL droplets roll off, whereas two of them remain pinned at any angle α. In Fig. S4 b) a plot of $\cos\theta_f - \cos\theta_b$ versus $\sin\alpha$ is presented. The dashed line is a fit of eq. (1) to the data using $\Delta F/F_{lv} = -0.04$ and $\rho Vg/F_{lv} = 0.67$. The liquid-vapor force F_{lv} is also here about 1.5 times the gravity, and the difference in solid-vapor and solid-liquid forces between the front and the back of the drop has opposite sign as compared for a pure stearic acid.

We have done measurements also for additional layers of coatings up to N=7 layers, and presented all the extracted values of $\rho Vg/F_{lv}$ in fig. 8 a). It appears that the liquid-vapor force F_{lv} decreases from $>2\rho Vg$ for a pure stearic acid layer to about $1.3\rho Vg$ for N=7. If one sets $F_{lv} = w\gamma_{lv}$ [27,36], with w an effective contact line length and γ_{lv} the liquid surface tension, the decrease in F_{lv} can be interpreted as a reduction in the effective contact line. This is not surprising, since while for a pure stearic acid coating the static contact angle is about 120°, adding layers of TiO_2 result in contact angles of the order of 150° and

therefore a reduced contact line length. For pure stearic acid surfaces $\cos\theta_b - \cos\theta_f > 1$, such that the $\theta_f > \theta_b$. For coatings with $N \geq 1$, $\Delta F/F_{lv}$ remains between -0.03 and -0.05 for $N \geq 1$, and is therefore not seen to vary much. Since the negative ΔF, corresponding to $\theta_f < \theta_b$, is observed in all measurements for all $N \geq 1$ when $\alpha \rightarrow 0°$, it appears that this is not only a coincidence due to the particular optical perspective used when observing the droplets. A full three-dimensional tomographic profile would indeed be helpful, but such a study is outside the scope of this work. Moreover, it does not explain that $\Delta F < 0$ when $\alpha \rightarrow 0°$ for the experiments on coated layers with $N \geq 1$, while $\Delta F > 0$ for stearic acid.

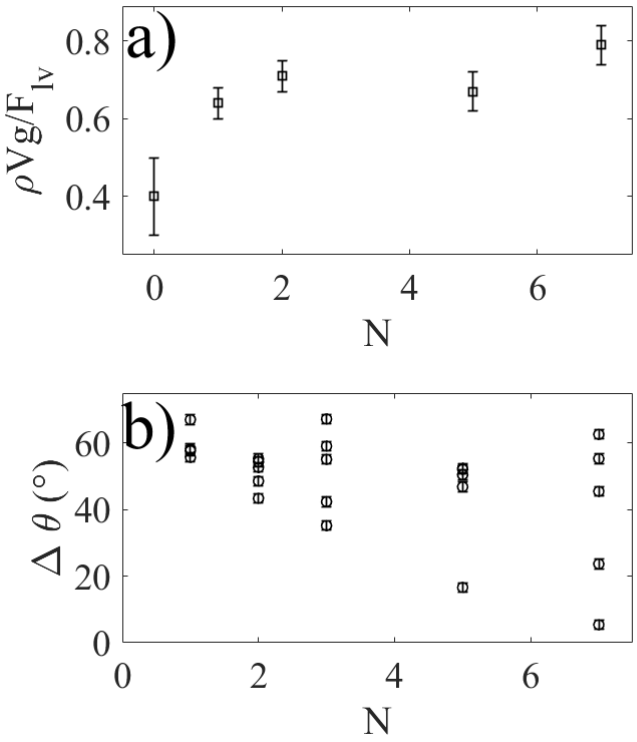

Figure 8. The ratio between gravity and liquid-vapor force ($\rho Vg/F_{lv}$) versus number of layers N (a). Here N=0 represent pure stearic acid. In b), the maximum difference in contact angle between front and back of a droplet for different layer thicknesses is shown. For each N, 5 measurements are reported, where some data points cannot be distinguished since they overlap.

It has been argued that a deposited droplet which is moved or vibrated will find a metastable contact angle not too far from equilibrium [26]. However, one might then expect a distribution of contact angles, and not the same sign of ΔF for every experiment. Recent theoretical analysis suggests that the advancing contact angle is always larger than the receding angle due to an entropic contribution [37]. However, it is not clear whether the conditions required in ref. [37] are fulfilled in the current experimental situation, since the contact line is trapped by the porous hydrophilic structure when $\alpha \rightarrow 0°$, and further theoretical investigations are needed to illuminate this issue. The reason for the switch from $\Delta F>0$ when $\alpha \rightarrow 0°$ for pure stearic acid to $\Delta F<0$ for a coating with $N \geq 1$ must somehow be related to the increased hydrophilicity and trapping that occurs when the oxide nanostructures are added, such that the front and back contact angles are trapped at $\theta_f < \theta_b$ when $\alpha \rightarrow 0°$. Further investigations on how the water penetrates into the coating is therefore needed, and detailed in the next section.

The data in Fig. 8 a) can also be put in connection with the observation shown in Fig. S4 a) that while some droplets stick to the surface and never move off (blue/red data points), others move off at tilt angles of about 60° (light green lines and dark green circles in Fig. S4 a)). When this happens, the maximum difference back and front contact angles is about 50°. Figure 8 b) shows the measured maximum difference in back and front contact angles, $\Delta\theta$, for different number of layers N. Each data point represents the value of $\Delta\theta$ found for an experiment similar to those in figs. 7 a) and S4 a), and 5 measurements are reported for each N. For example, for N=3, 5 different experiments are presented in fig. 8 b), and the measured $\Delta\theta$ took on values between 30 and 70°. For N=1 one finds $\Delta\theta$ to vary between 50° and 70°, whereas for N=7 the variation is between 5° and 65° for the 5 different measurements. For reference, pure stearic acid coating (N=0) has $\Delta\theta = 25 \pm 5°$, and 5 μL droplets do not move off the film at any tilt angle α. However, a pure stearic acid coating may not be a suitable comparison when it comes to $\Delta\theta$, since there are no TiO_2 nanostructures or heterogeneities, and has therefore not been included in Fig. 8 b).

The increase in variation in $\Delta\theta$ with number of coating layers as seen in Fig. 8 b) is accompanied by a reduced liquid-vapor force as seen in Fig. 8 a). However, also the possibility that the water drop may move off the surface increases with N. While N=1 and N=2 does not result in any droplets moving off the coating for any α, for N=7 the lowest roll-off angle of the droplets is $\alpha \approx 15°$. These observations are not surprising if the liquid-vapor force F_{lv}, and therefore also the effective contact line width w decreases as more coating layers are added.

Substrates with large adhesion most often exhibit large contact angle hysteresis, and this phenomenon has been studied extensively [38-45]. In our system, the surface coating is composed of small hydrophilic nanoparticles and larger stearic acid flakes, where we aim to obtain new understanding of how the water penetrates the porous hydrophilic regions to make direct contact with the copper surface. On a macroscopic scale, the coatings with different N appear parahydrophobic in the sense discussed in Ref. [4]. We noted that the droplets in our experiments in some cases did not move entirely off the surface, but merely moved a distance ranging from a few micrometers up to a centimeter before again coming to rest. The reason for this behavior is most likely found in the heterogeneity present on the surface, as seen in Fig. 2 and also in Fig. S1 and S2 in the supplementary information. Here it is seen that the surface with domains of hydrophilic TiO_2 nanoparticles are only partially covered by flakes of stearic acid. The domains of TiO_2 nanoparticles appear to be not well coated by stearic acid, i.e. there is a nano and microscale separation of hydrophilic and hydrophobic regions. The large contact angle is caused by the low surface energy of the stearic acid flakes, on which the three-phase contact line resides. The TiO_2 nanoparticle domain probably allow pinning of the contact line and prevent the droplets from moving off the surface.

Further elemental analysis using SEM-EDX are presented in Figs. 9 and S3 (supplementary information) for N=3 and N=5 layers respectively. It is observed that the carbon content associated with stearic acid is

relatively well distributed at N=3 as seen in Fig. 9 b), whereas the for N=5 it is more localized as observed from Fig. S3 b). The uniformity of carbon content for small N suggests that a thin layer of stearic acid is forming each time the substrate is dipped in this stearic acid, thus promoting large contact angles even at small N. However, for larger N more stearic acid flakes form, like those seen in fig. 2, and the EDX-signal from these probably overcome the signal from the uniform thin layer of stearic acid, therefore monitoring only the localized build-up of stearic acid flakes.

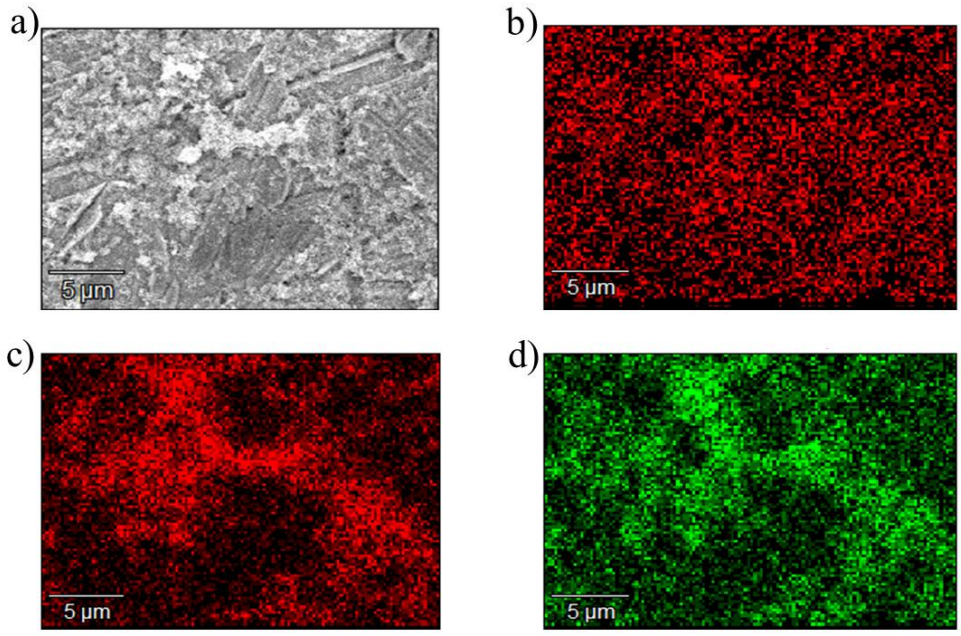

Figure 9. SEM EDX images of the TiO_2+stearic acid structure with N=3 layers.

a) is the total image, b) carbon, c) titanium and d) oxygen.

The titanium content associated with TiO_2 also becomes more uniformly distributed as the number of layers increase, as seen by comparing Figs. 9 c) and S3 c), which is reasonable as the density and uniformity of these nanoparticles increase when more layers are added. These observations may give further meaning to the wetting measurements above. For small N the droplets adhere to the surface and exhibit relatively large F_{lv} and possibly a larger contact line perimeter, similar to the case of pure stearic

acid. However, for larger N, the TiO_2 particles become more well-distributed, thus creating nanostructures that allow a thin stearic acid layer to form irregular films of high contact angle and gradually less contact area for the water drop to adhere to. Therefore, the water drops may more easily move off the film when tilting occurs.

The separation of stearic acid flakes and TiO_2 nanoparticles may also be a clue to explaining why the coatings remain stable over the time of the experiment. In fact, they were stored indoors for weeks before the experiments and the scanning electron microscope measurements without any apparent decline of the stearic acid flakes or alteration of wetting properties. It is well known that TiO_2 nanoparticles act as efficient photocatalytic agents in ultraviolet light [46,47]. Since the films used here were stored indoors under normal office and sunlight (through glass windows) conditions, they were exposed to some ultraviolet light, although no particular care was taken to measure how much. For degradation of stearic acid to occur via photocatalysis by TiO_2 nanoparticles, efficient transport of holes and electrons is needed. However, according to Figs. 2 and S3 (supplementary information) the nanoparticles are separated from the majority of the stearic acid domains, and no such efficient transport mechanisms appear to be available.

4. Electrical characterization of water penetration

Electrical transient current curves at constant potential were then recorded to shed further light on the initial contact between water and underlying copper surface. For the system studied here, is not possible to easily and accurately observe the water front penetrating the coating of TiO_2 nanoparticles and stearic acid on a copper surface using optical methods, since copper is not transparent and optical imaging through a curved water droplet surface (since the contact angle is very large) gives images of poor quality. However, the precise occurrence of electrical contact can be time-resolved by electrical characterization.

Figures 4 and 10 show the geometry used, where a 100 μL drop is resting on a bare, polished copper surface and then just brought in contact with a copper surface coated with stearic acid and TiO_2 nanoparticles. In this two-electrode configuration, the potential difference is maintained at V=0.5 V, while the current transient is measured, see Fig. 10 c).

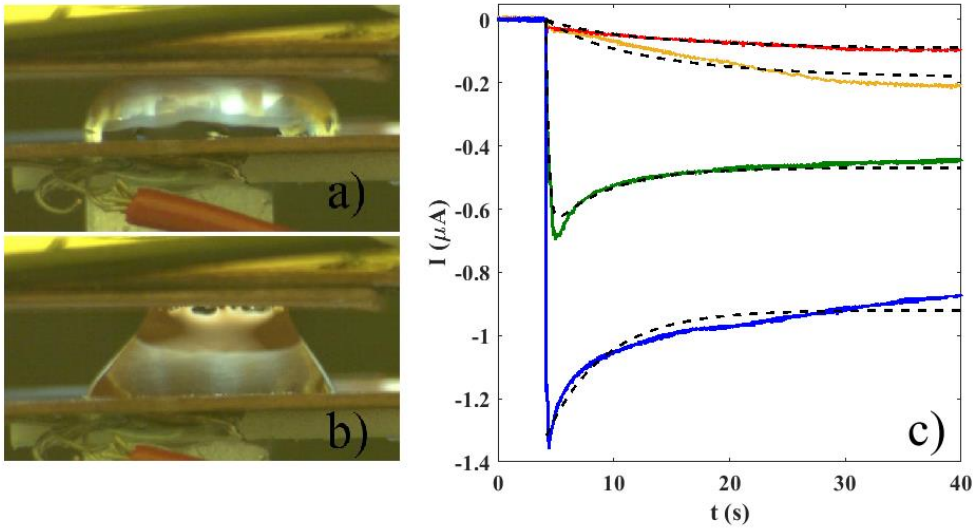

Figure 10. A droplet being squeezed between a bare copper electrode (lower) and a copper electrode coated with N=2 layers of TiO_2+stearic acid (upper), during a current transient (a) and upon withdrawal (b) after the experiment was completed. The current transients for a constant voltage of 0.5 V is shown for N=0 (blue), N=1 (green), N=2 (orange) and N=5 (red) in figure c). The dashed lines show fits to the experimental data as described in the text.

The lower electrode with the droplet resting on top was moved gradually such that it contacted the coated upper electrode. For each experiment, the stage was moved the same distance such that the current transient running through the electrodes did not change significantly upon repetition of the experiment (which was done at least three times for each sample). Using bare copper surfaces on both

electrodes, the current first quickly increased in about 0.2 s to -1.4 μA due to initiation of the redox reaction at the copper surface, see the blue curve in Fig. 10 c). Subsequently, the current decreased with time. A similar behavior is seen when the upper electrode is coated with N=1 layers of TiO_2 and stearic acid (green line), but now it took 0.8 s to reach the peak at about -0.7 μA before a decaying current transient was observed. For N=2 (orange line) and N=5 (red line) there was no peak, but rather a monotonous increase in current towards saturation. The time it takes to reach a quasi-equilibrium indicates that the layers of TiO_2 and stearic acid form a network which the water must penetrate in order to reach the copper surface. Note also that a small dip in current on the order of 10-100 nA was observed for all layers almost immediately after contact between droplet and coating, which could either be due to a nearly instant contact electrification of the coating or that it takes very short time for some small amount of the water to penetrate the thickness of the thin coating and down to the copper surface such that electrical contact is initiated. The initial water column connecting the copper electrodes through the layers of TiO_2 and stearic acid is believed to spread radially outwards in a nearly cylindrical geometry due to capillary pressure in the coating pores.

A simplified model for the current is set up by first assuming that the redox-reaction needed for nucleation happens very quickly [48], typically less than a second, such that the decay of the current seen for bare copper in Fig. 10 is due to the gradual depletion of ions from the water columns of the droplets. By subsequently assuming that the kinetics of the radial water movement is governed by a combination of capillary dynamics and evaporation [49-52], one obtains the following equation for the electrical current through the copper as a function of time (see the supplementing information for a detailed derivation)

$$I(t) = \pi c \tau \left(J_0 + \frac{\sigma_0}{\tau_A} e^{-t/\tau_A} \right) \left(1 - e^{-2t/\tau} \right) \quad . \qquad (2)$$

Here, $c=k\Delta p/\mu\phi$, k is the permeability (scaling with the pore size), μ is the viscosity of water, ϕ the porosity and Δp is the capillary pressure. The time constant $\tau=h\rho\phi/m_{ev}$ expresses the time taken to reach the radial limit of the water penetration, ρ is the mass density, where h is the coating film thickness and m_{ev} the evaporation rate per area. Moreover, τ_A is a measure of the time required for the ions to drift from the water drop reservoir to the copper surface, and J_0 is a constant that is a measure of the charge flux that becomes available as new copper surface area is created.

It must be emphasized that eq. (2) is only a simple approximation for the short-time current transients analyzed here, and that long-time transients may show an increase in current due to further creation of new area, droplet depinning, delayed redox-reactions, etc. The blue curve in Fig. 10 c) shows the current density on a bare copper surface. When fitting theory to the experimental data one assumes that the radius of the water in contact with copper remains constant during the experiment. The corresponding black dashed curve is a fit to the experimental data with $J_0\pi r_0^2$=-0.4 μA, $\pi r_0^2\sigma_0/\tau_A$=-0.9 μA and τ_A=5 s. These fitted parameters are in this study only used as reference when analyzing the coatings.

For a coating with N≥1 layers, r(t) is no longer constant and eq. (2) can be used directly. Note that the time constant τ_A is assumed independent of the coating and therefore remains the same as for bare copper. In Fig. 10 c), the black dashed line fitted to the data for N=1 (green line) corresponds to $c\tau=0.5r_0^2$ and τ=0.5 s, the black dashed line fitted to the data for N=2 (yellow line) corresponds to $c\tau=0.2r_0^2$and τ=20 s, whereas the black dashed line fitted to the data for N=5 (red line) corresponds to $c\tau=0.1r_0^2$ and τ=20 s.

The increase in characteristic time τ with film thickness (h) is expected as the number of layers (N) grow, which is observed as one goes from N=1 to N=2 but not from N=2 to N=5. On the other hand, $c\tau$ decreases from $0.5r_0^2$ to $0.1r_0^2$ as the number of layers increase from N=1 to N=5, thus reflecting the corresponding decrease in current with thicker coatings. This may be related to a reduction in

permeability or increase in evaporation rate as the thickness increases. The simple model provided here gives an explanation for the absence of current peaks as the number of coating layers increase. Instead, one observes a gradual increase in the current until it reaches a temporary peak, since the time scale of water displacement due to the gradual increase of r(t) is longer than that of the fast transients.

The data in Figs. 8 a) and fig. 10 c) may provide an explanation why $\Delta\theta$ in Fig. 8 b) shows greater variability and it is easier for small water drops to move off the coating as the number of coating layers increases. First, Fig. 8 a) suggests that the liquid-vapor force decreases when the number N increases. According to the electrical current measurements above, the maximum radius (proportional to the square root of $c\tau$) decreases as N increases, which means that there is less contact between the hydrophilic copper surface and water, caused by increased evaporation and physical barriers for water penetration through the thicker coatings. This may suggest that there are fewer adhesion points for the capillary water bridges, thus not allowing the water droplet to get a strong adhesion hold into the porous matrix and the copper surface. The adhesion is therefore smaller for larger number of coating layers, leading to the observations seen in Fig. 8.

We believe that the observations in Figs. 3, 8 and 10 together also provide a clue as to why ΔF is negative ($\theta_f < \theta_b$) for all $N \geq 1$ when $\alpha \rightarrow 0°$, but not for stearic acid. During the tilt when $\alpha \rightarrow 90°$, the front has a very large contact angle θ_f, such that more water is directly located above the coating in this position as seen in Fig. 3 b). Water penetrates into the nanostructured coating in front of the droplet, and becomes partially stuck and to varying degree contacts the copper surface directly. When the stage is tilted back to start such that $\alpha \rightarrow 0°$, the water that is stuck in the nanostructured coating is pinned, such that contact line remains fixed and thereby stretches the local droplet surface. The back side of the droplet does not experience the same stretching, since here θ_b is much closer to 90°, which means that the local pressure on the water to the left of the droplet into the porous network is smaller. The

corresponding contact angle θ_f is therefore smaller than θ_b when the plate again is approaching its horizontal position such that $\alpha \rightarrow 0°$.

The method featured here could be used to design coatings which allow almost spherical droplets to sit on surface and at the same time transfer water to the underlying surface, which may have applications in water harvesting or guidance of flow in microfluidic systems [3]. Ideally, the porous network should be able to transport the water as efficiently as possible. In our system this is taken care of by the TiO_2 nanoparticles, although the manner in which we let them self-assemble with stearic acid was not particularly optimized for fast fluid transport. At the same time, one would also like the underlying substrate to be strongly hydrophilic and to be able to contact the water as easily as possible. A drawback of the combination of TiO_2 nanoparticles and stearic acid used here is that the stearic acid has a low melting point (69 °C) and the entire coating is not very resistant to mechanical abrasion. Thus, one must search for more robust coatings for applications in harsh environments, but this is outside the scope of the current work.

5. Conclusion

We have created thin films with large apparent static contact angles by dip-coating polished copper in solutions of TiO_2 nanoparticles and terminated by stearic acid. The contact angle is studied using the tilted plate method. It is found that contact angles of horizontal water droplets at rest is about 150°, and that for layers of coating the droplets do not detach from the surface when tilted. When the number of coating layers increase, there adhesion to the surface diminishes, and there is a probability that the water droplets move off the surface. At the same time, it is also found that the liquid-vapor force is reduced, and that the front contact angle is larger than the back contact angle when the plate is tilted back into its original position. This was attributed to the formation of regions of TiO_2 and stearic acid nano and microstructures, as observed by scanning electron microscopy. Elemental analysis shows that the stearic acid forms a thin layer over the entire surface, but that as the number of coating layers are added there

are pronounced stearic acid flakes. Further electrical characterization demonstrates that the thinnest layers allow the water droplet to make quick contact with the underlying copper surface, whereas the process is slower and more limited for the coatings with many layers. These observations suggest that the adhesion of water drops to the thin coatings is enhanced by the liquid penetration into the porous network. Large adhesion appears to correlate with the ability of water to penetrate into the porous network to make contact with the underlying hydrophilic copper substrate. As the number of coating layers increase, the amount of water coming in contact with the copper is reduced, which may explain the reduced adhesion of water droplets observed in such situations. The experimental observations also suggest that the contact angle history is determined by the way the droplet is tilted, and results in asymmetric droplets when again put on a horizontal surface.

Our study demonstrates that porous solid films are interesting systems for controlling wetting properties depending on the manner in which the liquid penetrates into solid network, and the methods used here may find applications in studying such films.

Acknowledgements

This study was supported in part by the Nanostructure Laboratory at the Department of Physics and Technology, University of Bergen.

Data Availability

The data that support the findings of this study are available from the corresponding author upon reasonable request.

REFERENCES

(1) J.T. Simpson, S.R. Hunter og T. Aytug, "Superhydrophic materials and coatings: a review", Rep. Prog. Phys. **2015**, 78, 086501.

(2) W. Barthlott og C. Neinhus, "Purity of the sacred lotus, or escape from contamination in biological surfaces", Planta, **1997**, 202, 1-8.

(3) C.R. Szczepanski, F. Guittard and T. Darmanin, "Recent advances in the study and design of parahydrophobic surfaces: From natural examples to synthetic approaches", Advances in Colloid and Interface Science, **2017**, 241, 37-61.

(4) A. Marmur, C. Della Volpe, S.Siboni and A. Amirfazli, "Contact angles and wettability: towards common and accurate terminology", Surface Innovations, **2017**, 5, 3-8.

(5) C. Yuan, M. Huang, X. Yu, Y. Ma and X. Luo, "A simple approach to fabricate the rose petal-like hierarchical surfaces for droplet transportation", Appl. Surf. Sci., **2016**, 385, 562-568.

(6) R.N. Wenzel, "Resistance of solid surfaces to wetting by water", Ind. Eng. Chem., **1936**, 28, 988-994.

(7) A. Cassie and S. Baxter, "Wettability of porous surfaces", Trans. Faraday Soc., **1944**, 40, 546-551.

(8) E. Bormashenko, "Progress in understanding wetting transitions on rough surfaces", Advances in Colloid and Interface Science, **2015**, 222, 92-103.

(9) S.M. Hurst, B. Farschian, J. Choi, J. Kim and S. Park, "A universally applicable method for fabricating superhydrophobic polymer surfaces", Colloids and Surfaces A: Physiochem. Eng. Aspects, **2012**, 407, 85-90.

(10) J. Bravo, L. Zhai, Z. Wu, R.E. Cohen and M.F. Rubner, "Transparent superhydrophobic films based on silica nanoparticles", Langmuir, **2007**, 23, 7293-7298.

(11) Y.H. Lin, K.L. Su, P.S. Tsai, F.L. Chuang and Y.M. Yang, “Fabrication and characterization of transparent superhydrophilic/superhydrophobic silica nanoparticulate thin films”, Thin Solid Films, **2011**, 519, 5450-5455.

(12) Y. Hu, S. Huang, S. Liu and W. Pan, “A corrosion-resistance superhydrophobic TiO_2 film”, Appl. Surf. Sci., **2012**, 258, 7460-7464.

(13) M. Khazaei, M.T. Sadeghi and M.S. Hosseini, “Stable superhydrophilic coating on superhydrophobic porous media by functionalized nanoparticles”, Mater. Res. Express, **2018**, 5, 015019.

(14) M.S. Hosseini, M.T. Sadeghi and M. Khazaei, “Improving oleophobicity and hydrophilicity of superhydrophobic surface by TiO2 coatings”, Mater. Res. Express, **2018**, 5, 085010.

(15) Q. Wang, B. Zhang, M. Qu, J. Zhang and D. He, “Fabrication of superhydrophobic surfaces on engineering material surfaces with stearic acid”, Appl. Surface Science, **2008**, 254, 2009-2012.

(16) J. Zhu, “A novel fabrication of superhydrophobic surfaces on aluminium substrate”, Applied Surface Science, **2018**, 447, 363-367.

(17) B. Zhang, H. Feng, F. Lin, Y. Wang, L. Wang, Y. Dong and W. Li, “A facile process for preparing superhydrophobic nickel films with stearic acid”, Surface & Coatings Technology, **2013**, 231, 88-92.

(18) J. Zhu and X.F. Hu, “A novel and facile fabrication of superhydrophobic surfaces on copper substrate via machined operation”, Materials Letters, **2017**, 190, 115-118.

(19) Z. Wei, D. Jiang, J. Chen, S. Ren and L. Li, “Fabrication of mechanically robust superhydrophobic aluminum surface by acid etching and stearic acid modification”, J. Adhesion Sci. Technol, **2017**, 31, 2380-2397.

(20) R. Jain and R. Pitchumani, “Facile fabrication of durable copper-based superhydrophobic surfaces via electrodeposition”, Langmuir, **2017**, 34, 3159-3169.

(21) A.B. Gurav, S. S. Latthe, R.S. Vhatkar, J.G. Lee, D.Y. Kim, J.J. Park and S.S. Yoon, “Superhydrophobic surface decorated with vertical ZnO nanorods modified by stearic acid”, Ceramics International, **2014**, 40, 7151-7160.

(22) S. Maryam Shah, U. Zufiqar, S.Z. Hussain, I. Ahmad, H. Rehman, I. Hussain and T. Subhani, “A durable superhydrophobic coating for the protection of wood materials”, Materials Letters, **2017**, 203, 17-20.

(23) M.A. Arfaoui, P.I. Dolez, M. Dubé and É. David, “Preparation of a hydrophobic recycled jute-based nonwoven using a titanium dioxide/stearic acid coating”, The Journal of The Textile Institute, **2019**, 110, 16-25.

(24) M. Abbas, H. Iftikhar, M.H. Malik and A. Nazir, “Surface Coatings of TiO_2 nanoparticles onto the designed fabrics for enhanced self-cleaning properties”, Coatings, **2018**, 8, 35.

(25) A. Marmur, “The contact angle hysteresis puzzle”, Colloids Interfaces, **2022**, 6, 39.

(26) H.J. Bűtt, J. Liu, K. Koynov, B. Straub, C. Hinduja, I. Roismann, R. Berger, X. Li, D. Vollmer, W. Steffen and M. Kappl, “Contact angle hysteresis”, Curr. Opin. Coll. & Int. Sci., **2022**, 59, 101574.

(27) C.G.L Furmidge. “Studies at phase interfaces. I. The sliding of liquid drops on solid surfaces and a theory for spray retention”. Journal of Colloid Science, **1962**, 17.4, 309 –324.

(28) E. Pierce, F.J. Camora and A. Amirfazli, “Understanding of sliding and contact angle results in tilted plate experiments”, Colloids and Surfaces A, **2008**, 323, 73-82.

(29) B. Krasovitski and A. Marmur, “Drops down the hill: Theoretical study of limiting contact angles and hysteresis range on a tilted plate”, Langmuir, **2005**, 21, 3881-3885.

(30) R. Flatabø, A. Coste and M.M. Greve, “A systematic investigation of the charging effect in scanning electron microscopy for metal nanostructures on insulating substrates”, Journal of Microscopy, **2017**, 265, 287-297.

(31) P. Papadopoulos, L. Mammen, X. Deng, D. Vollmer and H.J. Bűtt, “How superhydrophobicity breaks down”,PNAS, **2013**, 110, 3254-3258.

(32) S.T. Larsen, N.K. Andersen, E. Søgaard and R. Taboryski, “Structure irregularity impedes drop roll-off at superhydrophobic surfaces”, Langmuir, **2014**, 30, 5041-5045.

(33) J.C. Berg, “An introduction to interfaces and colloids: The bridge to nanoscience”, World Scientific, 1st ed., **2010**.

(34) P.S. Swain and R. Lipowsky, “Contact angles on heterogenous surfaces: A new look at Cassie’s and Wenzel’s laws”, Langmuir, 1998, 14, 6772-6780.

(35) N.K. Adam and G. Jessop, “CCL.-Angles of contact and polarity of solid surfaces”, J. Chem. Soc., **1925**, 127, 1863-1868.

(36) N. Frøvik, M.M. Greve and L.E. Helseth, “Nanostructures and wetting properties controlled by reactive ion etching of fluorinated ethylene propylene”, Colloids and Surfaces A, **2019**, 574, 228-238.

(37) D.C. Standnes and P. Fotland, “On the importance of the entropic contribution to the Helmholtz free energy for the existence of contact angle hysteresis”, Colloid and Interface Science Communications, **2022**, 50, 100664.

(38) L. Feng, Y. Zhang, J. Xi, Y. Zhu, N. Wang, F. Xia and L. Jiang, "Petal effect: a superhydrophobic state with high adhesive force", Langmuir, **2008**, 24, 4114-4119.

(39) A. Winkleman, G. Gotesman, A. Yoffe and R. Naaman, "Immobilizing a drop of water: Fabricating highly hydrophobic surfaces that pin water droplets", Nano Lett., **2008**, 30, 1241-1245.

(40) E. Bormashenko, T. Stein, R. Pogreb and D. Aurbach, "Petal effect on surfaces based on Lycopodium: High-stick surfaces demonstrating high apparent contact angles", J. Phys. Chem. C, **2009**, 113, 5568-5572.

(41) X. Wang and R.A. Weiss, "A facile method for preparing sticky, hydrophobic polymer surfaces", Langmuir, **2012**, 28, 3298-3305.

(42) J.B.K. Law, A.M. H. Ng, A.Y. He and H.Y. Low, "Bioinspired Ultrahigh Water Pinning Nanostructures", Langmuir, **2014**, 301, 325–331.

(43) J. Wu, J. Xia, W. Lei and B.P. Wang, "Advanced understanding of stickiness on superhydrophobic surfaces", Scientific Reports, **2013**, 3, 3268.

(44) K. Grundke, K. Pöschel, A. Synytska, R. Frenzel, A. Drechsler, M. Nitschke, A.L. Cordeiro, P. Uhlmann and P.B. Welzel, "Experimental studies of contact angle hysteresis phenomena on polymer surfaces — Toward the understanding and control of wettability for different applications", Adv. Coll. Interface Sci., **2015**, 222, 350-376.

(45) B. Balu, V. Breedveld and D.W. Hess, "Fabrication of "roll-off" and "sticky" superhydrophobic cellulose surfaces via plasma processing", Langmuir, **2008**, 24, 4785-4790.

(46) S. Alofi, C. O'Rourke and A. Mills, "Modelling the kinetics of stearic acid destruction on TiO2 'self-cleaning' photocatalytic films", Applied Catalysis A, **2022**, 647, 118899.

(47) S. Alofi, C. O'Rourke and A. Mills, "Photocatalytic destruction of stearic acis by TiO2 film: Evidence of highly efficient transport of photogenerated electrons and holes", Journal of Photochemistry & Photobiology A, **2023**, 435, 114273.

(48) A.S. Gliozzi, A.L. Alexe-Ionescu and G. Barbero, "Ohmic model for electrodeposition of metallic ions", Phys. Lett. A, **2015**, 379, 2657-2660.

(49) R. Lucas, "Über das Zeitgesetz des kapillaren Aufstiegs von Flüssigkeiten", Kolloid-Z, **1918**, 23, 15-22

(50) E.W. Washburn, "The dynamics of capillary flow", Phys. Rev., **1921**, 17,273-283

(51) A. Rogacs, J.E. Steibrenner, J.A. Rowlette, J.M. Weisse, X.L. Zheng and K.E. Goodson, J. Coll. Interface Sci., **2010**, 349, 354-360.

(52) M. Mercuri, K. Pierpauli, M.G. Bellino and C.L.A. Berli, "Complex filling dynamics in mesoporous thin films", Langmuir, **2017**, 33, 152-157.